Nonlinear Dyn
https://doi.org/10.1007/s11071-021-06534-9

ORIGINAL PAPER

Analytical solutions of solitary waves and their collision stability in a pre-compressed one-dimensional granular crystal

Zhi-Guo Liu · Jinliang Zhang · Yue-Sheng Wang · Guoliang Huang

Received: 2 March 2021 / Accepted: 10 May 2021

Abstract In this paper, a pre-compressed one-dimensional granular crystal model is studied. The bright analytic single and multiple solitary wave solutions in more general forms than those obtained the KdV system in the previous studies are derived by using the homogeneous balance principle and Hirota's bilinear method. The difference between the present solutions and those from the KdV system are investigated both analytically and numerically. By analyzing the dispersion relation and the collision process of solitary waves, we find that there are two types of double-solitary waves in the pre-compressed granular crystal model. The geometric and numerical analysis of dynamic behaviors of the solutions is presented with emphasis on the relation between the double-solitary waves and elastic collision between single-solitary waves. We find that the opposite collision between single-solitary waves may be stable and thus generate a stable double-solitary wave. It is concluded that the collision is a special stable double-solitary wave solution. We further propose a possible way to determine the stability of multiple solitary waves qualitatively. The results of this paper provide a theoretical basis for finding stable multiple solitary wave solutions.

Keywords Nonlinear waves · Multiple solitary waves · Stability · Granular crystal

1 Introduction

One distinguishing feature of wave propagation in a linear periodic structure (also termed phononic crystal) is the appearance of "stop bands" [1, 2], which can be used to control the propagation of waves. These stop bands allow phononic crystals to serve as mechanical filters [3], waveguides [4, 5], diodes [6–9] and resonators [10]. Although we have found a lot of interesting phenomena and extensive applications in linear phononic crystals, nonlinear phononic crystals have attracted much attention in recent years due to their tunable phononic characteristics [11]. Moreover, nonlinear phononic crystals have some phenomena that linear phononic crystals do not have, such as solitons [12–14] and second harmonic [15].

Z.-G. Liu · J. Zhang
School of Mathematics & Statistics, Henan University of Science & Technology, Luoyang 471000, China

Z.-G. Liu · Y.-S. Wang (✉)
Department of Mechanics, Beijing Jiaotong University, Beijing 100044, China
e-mail: yswang@bjtu.edu.cn; yswang@tju.edu.cn

Y.-S. Wang
Department of Mechanics, School of Mechanical Engineering, Tianjin University, Tianjin 300350, China

G. Huang
Department of Mechanical and Aerospace Engineering, University of Missouri, Columbia, MO 65211, USA

Published online: 26 May 2021

Elastic wave interaction with nonlinear phononic crystals yields some fascinating phenomena, among which solitary waves phenomena have been studied most intensively, namely discrete breathers [16–19], highly nonlinear solitary waves [20–22]. They feature unique properties as well as potential for applications, e.g., novel granular protection systems [23] and nonlinear phononic crystal waveguide [24, 25].

The simplest case of nonlinear phononic crystals is one-dimensional granular chain of mass [26]. The Fermi–Pasta–Ulam (FPU) problem was proposed from such nonlinear systems by Fermi et al. [27]. Later, the Korteweg-de Vries (KdV) equation [28] was derived from the FPU lattice. The soliton solution for the KdV equation explains the FPU problem under certain conditions. There are not only single solitons but also multiple solitons in KdV equation, which makes it very important in describing the dynamic behavior of weakly nonlinear systems. It should be noted that in the long wavelength approximation, the discrete system (e.g., the granular chains) can be described by KdV (or m-KdV) equation [26]. The FPU chain is a model for nearest neighbor coupled with harmonic plus cubic (or quartic) nonlinear interactions. The long wavelength approximation gives rise to a Boussinesq equation or a nonlinear Schrodinger (NLS) equation which admit soliton solutions. Certain studies have also employed this approximation [29].

Granular crystals consisting of tightly packed aggregates of particles in a periodic arrangement have evinced special interest due to their tunable nonlinear [26]. It is shown that the interactions between spheres are highly nonlinear under weak pre-compression but are weakly nonlinear under higher pre-compression. Recently, these nonlinear systems have been studied extensively as they can be used as an ideal experimental platform for the study of interplay between discrete and continuum systems. There are a lot of mathematical methods for studying wave phenomena in nonlinear continuous systems, such as the perturbation techniques [30, 31]. However, discrete nonlinear systems have received little attention. Due to the complexity of discrete systems, the research methods are mostly focused on numerical simulation. And the study of discrete systems based on analytical solutions is very few.

In this paper, the continuous equation corresponding to the discrete granular system, namely Boussinesq equation [29], is studied by solving the equation analytically. Then, the analytical solution is used as the initial signal to study the dynamic behavior and stability of the solution of the original discrete granular system. In Ref. [32], a continuous equation (Eq. (2.3) in Ref. [32], which belongs to Boussinesq equation [29]) in the original system without coordinate transformation was obtained in an initially compressed chain of granular spheres. In Ref. [33], we obtained the exact analytical single-solitary wave solution from this continuous equation (Eq. (6) in Ref. [33]). However, only approximate analytical solutions of multiple solitary waves were constructed without rigorous mathematical derivation. Moreover, there are some restrictions on the solutions, e.g., they do not hold when the wavenumbers of arbitrary two single-solitary waves are opposite. In order to resolve the above problems, the bilinear method and homogeneous balance principle are suggested to solve the continuous equation directly. Based on the obtained analytical solutions, the dynamic behavior and stability of the double-solitary wave are studied in detail.

2 Continuous equation and analytical solutions

Consider a granular chain of identical spheres with mass m pre-compressed by a static load F_0, see Fig. 1 where $\tilde{\delta}_0$ is the compression under the preset static load.

The governing equation for a monatomic granular chain of spherical particles under the pre-compression $\tilde{\delta}_0$ can be written as [32]

$$\ddot{\tilde{u}}_i = A(\tilde{\delta}_0 - \tilde{u}_i + \tilde{u}_{i-1})^{3/2} - A(\tilde{\delta}_0 - \tilde{u}_{i+1} + \tilde{u}_i)^{3/2}, \tag{1}$$

where $\tilde{u}_i$ indicates the displacements of the ith spheres with the superscripted dot denoting the derivation w.r.t time $\tilde{t}$, and the Hertzian constant $A = \frac{E(2\tilde{R})^{1/2}}{3m(1-\upsilon_m^2)}$ [32] with $\tilde{R}$, m, E and υ_m being the radius, mass, Young's modulus and Poisson's ratio of the spheres, respectively.

For convenience of discussion, we deal with the governing Eq. (1) in the dimensionless form. To this end, we set L to be a given characteristic length scale and introduce the following dimensionless variables:

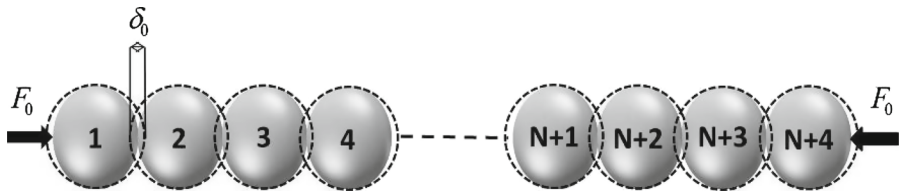

Fig. 1 Schematic diagram of the granular chain of identical elastic spheres pre-compressed by a static load [33]

$$u_n = \tilde{u}_n/L,\ t = \tilde{t}\sqrt{L^{1/2}A}, \tag{2}$$

and three dimensionless parameters

$$\delta_0 = \tilde{\delta}_0/L,\ R = \tilde{R}/L. \tag{3}$$

Then Eq. (1) can be transformed into the following dimensionless equation in terms of the dimensionless variables and parameters:

$$\ddot{u}_i = (\delta_0 - u_i + u_{i-1})^{3/2} - (\delta_0 - u_{i+1} + u_i)^{3/2}. \tag{4}$$

It should be indicated that the superscripted dot in the above equation represents the derivation w.r.t the dimensionless time t.

Using the long-wave approximation [32], we can write Eq. (4) in a continuous form:

$$u_{tt} - c_0^2 u_{xx} - 2c_0\gamma u_{xxxx} + \varepsilon u_x u_{xx} = 0, \tag{5}$$

where $c_0^2 = 6R^2\delta_0^{1/2}$; $\gamma = c_0R^2/6$; $\varepsilon = c_0^2R/\delta_0$; and x is the dimensionless special coordinate.

Equation (5) belongs to Boussinesq equation [29] and can be solved by using the homogeneous balance principle [35–38]. To this end, we can assume that the derivation of the solution to Eq. (5) w.r.t x is

$$u = -A_1\frac{\partial(\ln f)}{\partial x},\ v = \frac{\partial u}{\partial x},\ A_1 = \frac{24c_0\gamma}{\varepsilon}. \tag{6}$$

Substituting Eq. (6) into Eq. (5), we can obtain

$$\begin{aligned} &-A_1(\ln f)_{,xtt} + c_0^2A_1(\ln f)_{,xxx} + 2c_0\gamma A_1(\ln f)_{,xxxxx} \\ &\quad + \varepsilon A_1^2(\ln f)_{,xx}(\ln f)_{,xxx} \\ &\quad = 0. \end{aligned} \tag{7}$$

To reduce the calculation, we integrate Eq. (7) w.r.t x by setting the integral constant to be zero and then have

$$\begin{aligned} &(\ln f)_{,tt} - c_0^2(\ln f)_{,xx} - 2c_0\gamma(\ln f)_{,xxxx} \\ &\quad - \frac{A_1\varepsilon}{2}\left[(\ln f)_{,xx}\right]^2 \\ &\quad = 0. \end{aligned} \tag{8}$$

Considering the following relations:

$$\begin{cases} \frac{\partial^2(lnf)}{\partial t^2} = \frac{1}{f^2}\left[-(f_{,t})^2 + ff_{,tt}\right], \\ \frac{\partial^2(lnf)}{\partial x^2} = \frac{1}{f^2}\left[-(f_{,x})^2 + ff_{,xx}\right], \\ \frac{\partial^4(lnf)}{\partial x^4} = \frac{1}{f^4}\left[-3f^2(f_{,xx})^2 - 4f^2f_{,x}f_{,xxx} + 12f(f_{,x})^2f_{,xx} - 6(f_{,x})^4 + f^3f_{,xxxx}\right], \end{cases} \tag{9}$$

we can rewrite Eq. (8) as

$$\begin{aligned} &\left[-(f_{,t})^2 + ff_{,tt}\right] - c_0^2\left[-(f_{,x})^2 + ff_{,xx}\right] \\ &- 2c_0\gamma\left[-3(f_{,xx})^2 - 4f_{,x}f_{,xxx} + ff_{,xxxx}\right] \\ &\quad - \frac{A_1\varepsilon}{2}(f_{,xx})^2 - 2c_0\gamma\left[\frac{12}{f}(f_{,x})^2f_{,xx} - \frac{6}{f^2}(f_{,x})^4\right] \\ &+ \frac{A_1\varepsilon}{2}\left[-\frac{1}{f^2}(f_{,x})^4 + \frac{2}{f}f_{,xx}(f_{,x})^2\right] = 0, \end{aligned} \tag{10}$$

which can be denoted as the following simple form by using the properties of Hirota bilinear [39]:

$$D_t^2(f\cdot f) - c_0^2D_x^2(f\cdot f) - 2c_0\gamma D_x^4(f\cdot f) = 0, \tag{11}$$

where D is the Hirota bilinear operator defined as [34]

$$\begin{aligned} &D_t^mD_x^nD_y^kD_z^l(g\cdot h) \\ &= \left(\frac{\partial}{\partial t} - \frac{\partial}{\partial t'}\right)^m\left(\frac{\partial}{\partial x} - \frac{\partial}{\partial x'}\right)^n\left(\frac{\partial}{\partial y} - \frac{\partial}{\partial y'}\right)^k\left(\frac{\partial}{\partial z} - \frac{\partial}{\partial z'}\right)^l(g\cdot h)\Big|_{x=x',y=y',z=z',t=t'}. \end{aligned}$$

Equation (11) can be solved by using Hirota's bilinear method. Expand f into a power series of a small parameter ε:

$$f(x,t) = \sum_{n=0}^{+\infty} f_n(x,t)\varepsilon^n, \tag{12}$$

which when substituted into Eq. (11) yields

$$(D_t^2 - c_0^2 D_x^2 - 2c_0\gamma D_x^4)\left(\sum_{n=0}^{+\infty} f_n(x,t)\varepsilon^n \cdot \sum_{n=0}^{+\infty} f_n(x,t)\varepsilon^n\right) = \sum_{n=0}^{+\infty} \varepsilon^n (D_t^2 - c_0^2 D_x^2 - 2c_0\gamma D_x^4)\left(\sum_{m+l=n} f_m \cdot f_l\right). \tag{13}$$

Setting the coefficient of the term for each order of ε in Eq. (14) to be zero, we obtain

$$\left(D_t^2 - c_0^2 D_x^2 - 2c_0\gamma D_x^4\right)\left(\sum_{m+l=n} f_m \cdot f_l\right) = 0,\ n = 0,1,2,\ldots, \tag{14}$$

of which the first four equations are

$$(D_t^2 - c_0^2 D_x^2 - 2c_0\gamma D_x^4)(f_0 \cdot f_0) = 0, \tag{15}$$

$$(D_t^2 - c_0^2 D_x^2 - 2c_0\gamma D_x^4)(f_1 \cdot f_0) = 0, \tag{16}$$

$$2(D_t^2 - c_0^2 D_x^2 - 2c_0\gamma D_x^4)(f_2 \cdot f_0) + (D_t^2 - c_0^2 D_x^2 - 2c_0\gamma D_x^4)(f_1 \cdot f_1) = 0, \tag{17}$$

$$2(D_t^2 - c_0^2 D_x^2 - 2c_0\gamma D_x^4)(f_3 \cdot f_0) + 2(D_t^2 - c_0^2 D_x^2 - 2c_0\gamma D_x^4)(f_2 \cdot f_1) = 0. \tag{18}$$

It is noted that Eqs. (15)–(18) are a set of recurrence equations. To solve f_n for $n > 1$, we should first have a solution of f_0 (i.e., the first term of Eq. (12)). Theoretically speaking, we can take any solution of f_0 which satisfies Eq. (15). Without of loss of generality, we follow Ref. [34] and assume f_0 to be a constant. Then Eq. (16) has an exponential eigen-solution:

$$f_1 = \mathrm{e}^{kx+\omega t+\delta}, \tag{19}$$

where k and ω may be interpreted as the wavenumber and angular frequency, respectively, and δ is an arbitrary constant. Substitution of (19) into Eq. (16) yields

$$(\omega^2 - c_0^2 k^2 - 2c_0\gamma k^4) f_0 f_1 = 0. \tag{20}$$

from which we obtain the dispersion relation:

$$\omega^2 - c_0^2 k^2 - 2c_0\gamma k^4 = 0. \tag{21}$$

The sum of the eigen-solution, Eq. (19), w.r.t all or partial possible values of j ($j = 1 \cdots N$) also satisfies Eq. (16). Therefore, we have the following eigen-solution:

$$f_1 = \sum_{j=1}^{N} \mathrm{e}^{\theta_j},\ \theta_j = k_j x + \omega_j t + \delta_j. \tag{22}$$

Substitution of Eq. (22) into Eq. (17) yields

$$\begin{aligned} &2(D_t^2 - c_0^2 D_x^2 - 2c_0\gamma D_x^4)(f_2 \cdot f_0) \\ &= -(D_t^2 - c_0^2 D_x^2 - 2c_0\gamma D_x^4)\left(\sum_{i=1}^{N} \mathrm{e}^{\theta_i} \cdot \sum_{j=1}^{N} \mathrm{e}^{\theta_j}\right) \\ &= -\sum_{i=1}^{N}\sum_{j=1}^{N}\left[(\omega_i - \omega_j)^2 - c_0^2(k_i - k_j)^2 - 2c_0\gamma(k_i - k_j)^4\right]\mathrm{e}^{\theta_i+\theta_j} \\ &= -2\sum_{1\le i<j\le N}\left[(\omega_i - \omega_j)^2 - c_0^2(k_i - k_j)^2 - 2c_0\gamma(k_i - k_j)^4\right]\mathrm{e}^{\theta_i+\theta_j}, \end{aligned} \tag{23}$$

from which we obtain

$$f_2 \cdot f_0 = \sum_{1\le i<j\le N} A_{ij}\mathrm{e}^{\theta_i+\theta_j}, \tag{24}$$

where

$$A_{ij} = \frac{(\omega_i - \omega_j)^2 - c_0^2(k_i - k_j)^2 - 2c_0\gamma(k_i - k_j)^4}{-(\omega_i + \omega_j)^2 + c_0^2(k_i + k_j)^2 + 2c_0\gamma(k_i + k_j)^4}, (i,j = 1,2,3). \tag{25}$$

Following the same process, we can obtain

$$f_3 \cdot f_0 = -\sum_{\substack{1\le i<j\le N \\ 1\le l\le N}} \frac{(\omega_i - \omega_j)^2 - c_0^2(k_i - k_j)^2 - 2c_0\gamma(k_i - k_j)^4}{(\omega_i + \omega_j)^2 - c_0^2(k_i + k_j)^2 - 2c_0\gamma(k_i + k_j)^4}\mathrm{e}^{\theta_i+\theta_j+\theta_l}. \tag{26}$$

All the other terms, f_i ($i = 4,\ldots,N$), can be derived similarly. Substituting f_i into Eq. (12) with the result inserted into Eq. (6), we can obtain the solutions to Eq. (5). Here we present the detailed expressions of the specific solutions for N = 1,2,3,4 with $\varepsilon = 1$. (This is not out of generality because we have $\varepsilon = \mathrm{e}^{\ln\varepsilon}$ which can be included into the exponent of the exponential function, for details we refer to Ref. [40].)

(1) The bright single-solitary wave solution

When N = 1, we set $f_2 = 0$ and $f_0 = 1$ and then have $f = f_0 + f_1 = 1 + \mathrm{e}^{\theta_1}$ with $\theta_1 = k_1\xi - \omega_1\tau$ (where $\delta_1 = 0$ is assumed). Finally, we can obtain, from Eq. (6), the single-solitary wave solution

$$v_1(x,t) = -A_1\frac{k_1^2\mathrm{e}^{\theta_1}}{(1+\mathrm{e}^{\theta_1})^2}, \tag{27}$$

where $\omega_1^2 = c_0^2 k_1^2 + 2c_0\gamma k_1^4$.

(2) The bright double-solitary wave solution

When $N = 2$, we set $f_3 = 0$ and $f_0 = 1$, and then have $f = f_0 + f_1 + f_2 = 1 + e^{\theta_1} + e^{\theta_2} + A_{12}e^{\theta_1+\theta_2}$ with $\theta_i = k_i\xi - \omega_i\tau$ (where $\delta_i = 0$ is assumed). Finally, we can obtain, from Eq. (6), the double-solitary wave solution

$$v_2(x,t) = -A_2\frac{k_1^2e^{\theta_1} + k_2^2e^{\theta_2} + 2(k_1-k_2)^2e^{\theta_1+\theta_2} + A_{12}(k_2^2e^{2\theta_1+\theta_2} + k_1^2e^{\theta_1+2\theta_2})}{(1+e^{\theta_1}+e^{\theta_2}+A_{12}e^{\theta_1+\theta_2})^2}, \tag{28}$$

where $A_2 = A_1$; $\omega_i^2 = c_0^2k_i^2 + 2c_0\gamma k_i^4$ $(i = 1, 2)$; and

$$A_{12} = \frac{(\omega_1-\omega_2)^2 - c_0^2(k_1-k_2)^2 - 2c_0\gamma(k_1-k_2)^4}{-(\omega_1+\omega_2)^2 + c_0^2(k_1+k_2)^2 + 2c_0\gamma(k_1+k_2)^4}. \tag{29}$$

The other multiple solitary wave solutions to Eq. (5) can be obtained similarly. For instance, the triple- and quadruple-solitary wave solutions are

$$\begin{aligned} v_3(x,t) = -A_3\frac{\partial^2}{\partial\xi'^2}\ln[1 + e^{\theta_1} + e^{\theta_2} + e^{\theta_3} + A_{12}e^{\theta_1+\theta_2} \\ + A_{13}e^{\theta_1+\theta_3} + A_{23}e^{\theta_2+\theta_3} + A_{12}A_{13}A_{23}e^{\theta_1+\theta_2+\theta_3}], \end{aligned} \tag{30}$$

and

$$v_4(x,t) = -A_4\frac{\partial^2}{\partial\xi'^2}\ln[\Lambda(x,t)], \tag{31}$$

with $A_4 = A_3 = A_1$,

$$\begin{aligned} \Lambda(\xi',\tau) = 1 &+ e^{\theta_1} + e^{\theta_2} + e^{\theta_3} + e^{\theta_4} + A_{12}e^{\theta_1+\theta_2} \\ &+ A_{13}e^{\theta_1+\theta_3}A_{14}e^{\theta_1+\theta_4} + A_{23}e^{\theta_2+\theta_3} \\ &+ A_{24}e^{\theta_2+\theta_4} + A_{34}e^{\theta_3+\theta_4} \\ &+ A_{12}A_{13}A_{23}e^{\theta_1+\theta_2+\theta_3} \\ &+ A_{12}A_{14}A_{24}e^{\theta_1+\theta_2+\theta_4} \\ &+ A_{12}A_{14}A_{34}e^{\theta_1+\theta_3+\theta_4} \\ &+ A_{23}A_{24}A_{34}e^{\theta_2+\theta_3+\theta_4} \\ &+ A_{12}A_{13}A_{14}A_{23}A_{24}A_{34}e^{\theta_1+\theta_2+\theta_3+\theta_4} \end{aligned} \tag{32}$$

$$A_{ij} = \frac{(\omega_i-\omega_j)^2 - c_0^2(k_i-k_j)^2 - 2c_0\gamma(k_i-k_j)^4}{-(\omega_i+\omega_j)^2 + c_0^2(k_i+k_j)^2 + 2c_0\gamma(k_i+k_j)^4}, \quad (i,j = 1,2,3,4). \tag{33}$$

To some extent, the solitary wave solutions obtained above and the asymptotic solutions constructed in Ref. [33] (see Eqs. (30)–(33) therein) are different representations of the same physical phenomenon. It is indeed not difficult to verify that the derivations of the solutions in Ref. [33] w.r.t the space coordinate x are the same as the bright solitary wave solutions (27)–(31). However, we find that the coefficient A_{ij} in the present multiple solitary wave solutions and those in Ref. [33] are different. To avoid confusion, denote A_{ij} in Ref. [33] as $\overline{A}_{ij}$.

Figure 2 presents the curves of A_{12} and $\overline{A}_{12}$ varying with k_2 for $k_1 = 1, c_0 = 1$, and $\gamma = 0.5$. Two situations, $\omega_1 \cdot \omega_2 > 0$ and $\omega_1 \cdot \omega_2 < 0$, are shown in Fig. 1a and b, respectively. Discrepancy between A_{12} and $\overline{A}_{12}$ is observed in Fig. 1a near the point $k_2 = -k_1(= -1)$ where $\overline{A}_{12}$ is infinite, while A_{12} is finite. As k_2 becomes far away from this point, A_{12} and $\overline{A}_{12}$ are close to each other. In Fig. 2b for $\omega_1 \cdot \omega_2 < 0$, A_{12} and $\overline{A}_{12}$ are in good agreement even at the point $k_2 = -k_1(= -1)$. Similar results can be obtained for other A_{ij} $(i, j = 1,2,3,4)$.

The above analysis implies that there are two types of double-solitary waves ($k_1 \cdot k_2 < 0$ and $k_1 \cdot k_2 > 0$) in Eq. (5), but not in KdV equation [33]. This is the most important difference between the double-solitary wave solutions obtained in the present paper and Ref. [33]. The similar conclusion is applicable to other multiple solitary wave solutions. In general, the multiple solitary wave solutions in this paper have more general forms (including the case of $k_i + k_j = 0$) than those obtained in Ref. [33].

By integrating Eq. (27) w.r.t x, the corresponding dark single-solitary wave solution can be obtained:

$$u_1(x,t) = -A_1\frac{k_1e^{\theta_1}}{1+e^{\theta_1}}. \tag{34}$$

Although it seems that the corresponding dark multiple solitary wave solutions can be obtained by integrating the bright ones (Eqs. (28), (30) and (31)) based on the relation $v = \partial u/\partial x$, it is not easy to obtain the closed-form expressions. However, as we mentioned above, the derivation of the multiple solitary wave solutions in Ref. [33] (Eqs. (31)–(33)) w.r.t x is the same as the solutions, Eqs. (28), (30) and (31), in form. Therefore, we can directly write the dark multiple solitary wave solutions corresponding to the

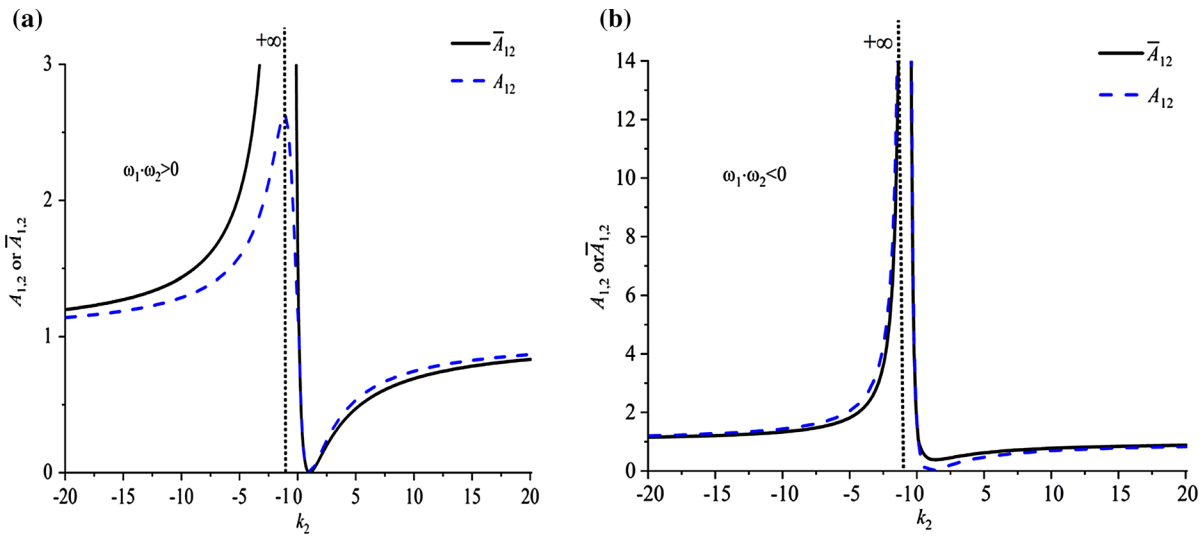

Fig. 2 Comparison of A_{12} and $\bar{A}_{12}$ with $c_0 = 1$, $\gamma = 0.5$ and $k_1 = 1$

bright ones (Eqs. (28), (30) and (31)). For example, the dark double-solitary wave solution is

$$u_2(x,t) = -A_2\frac{k_1\mathrm{e}^{\theta_1} + k_2\mathrm{e}^{\theta_2} + A_{12}(k_1+k_2)\mathrm{e}^{\theta_1+\theta_2}}{1+\mathrm{e}^{\theta_1}+\mathrm{e}^{\theta_2}+A_{12}\mathrm{e}^{\theta_1+\theta_2}} + C, \tag{35}$$

where C is a constant; and A_{12} is given by Eq. (29). The other dark multiple solitary wave solutions can be obtained similarly.

In addition, the multiple solitary wave solutions obtained here still have the dynamic characteristics of the solutions to the KdV equation described in Ref.[33], that is, in some limiting cases [$\mathrm{e}^{\theta_i} \approx 1$, $\mathrm{e}^{\theta_j} \ll 1$ $(i \neq j)$], the multiple solitary wave solutions reduce approximately to single-solitary wave solutions (θ_i-single-solitary waves). Particularly, for the double-solitary wave solution, we have.

(i) $\mathrm{e}^{\theta_1} \approx 1$ and $\mathrm{e}^{\theta_2} \ll 1$. In this case, we can remove e^{θ_2}-independent terms by setting $\mathrm{e}^{\theta_2} \approx 0$. Then Eq. (35) becomes

$$\begin{aligned} u_2(x,t) &= -A_2\frac{k_1\mathrm{e}^{\theta_1}+k_2\mathrm{e}^{\theta_2}+A_{12}(k_1+k_2)\mathrm{e}^{\theta_1+\theta_2}}{1+\mathrm{e}^{\theta_1}+\mathrm{e}^{\theta_2}+A_{12}\mathrm{e}^{\theta_1+\theta_2}} + C \approx -A_2k_1\frac{\mathrm{e}^{\theta_1}}{1+\mathrm{e}^{\theta_1}} + C \\ &= -\frac{1}{2}A_2k_1\left(\frac{\mathrm{e}^{\theta_1}-1}{\mathrm{e}^{\theta_1}+1}\right) + C_1 = -\frac{1}{2}A_2k_1\tanh\frac{\theta_1}{2} + C_1, \end{aligned} \tag{36}$$

where C_1 is a constant.

(ii) $\mathrm{e}^{\theta_1} \ll 1$ and $\mathrm{e}^{\theta_2} \approx 1$. In this case, we can remove e^{θ_1}-independent terms by setting $\mathrm{e}^{\theta_1} \approx 0$. Then Eq. (35) becomes

$$\begin{aligned} u_2(x,t) &= -A_2\frac{k_1\mathrm{e}^{\theta_1}+k_2\mathrm{e}^{\theta_2}+A_{12}(k_1+k_2)\mathrm{e}^{\theta_1+\theta_2}}{1+\mathrm{e}^{\theta_1}+\mathrm{e}^{\theta_2}+A_{12}\mathrm{e}^{\theta_1+\theta_2}} + C \\ &\approx -\frac{1}{2}A_2k_2\tanh\frac{\theta_2}{2} + C_1. \end{aligned} \tag{37}$$

From these two limiting cases, we can see that the dark double-solitary waves can degenerate into two dark single-solitary waves. Similarly, according to the above result, we can combine two single-solitary waves into a double-solitary wave in a certain way. In other words, the multiple solitary waves can be regarded as elastic collision between single-solitary waves. This provides us a way to excite multiple solitary waves using single-solitary waves.

In order to further understand the dynamic characteristics of the bright and dark solitary waves, we investigate their characteristics in space–time domain, frequency–wavenumber domain, frequency–space domain, and time–wavenumber domain. Figures 3 and 4 show the corresponding results of the bright and dark single-solitary wave solutions, respectively.

A bright single-solitary wave evolving in the space–time domain is observed in Fig. 3a. Its dispersion curve shown Fig. 3b is evolved in a region around an oblique line passing through the zero point. Figure 3c and d describes the dynamic energy flow in the evolution process in the space–frequency domain and the time–wavenumber domain, respectively. It is easy to see from the color scale bar that the

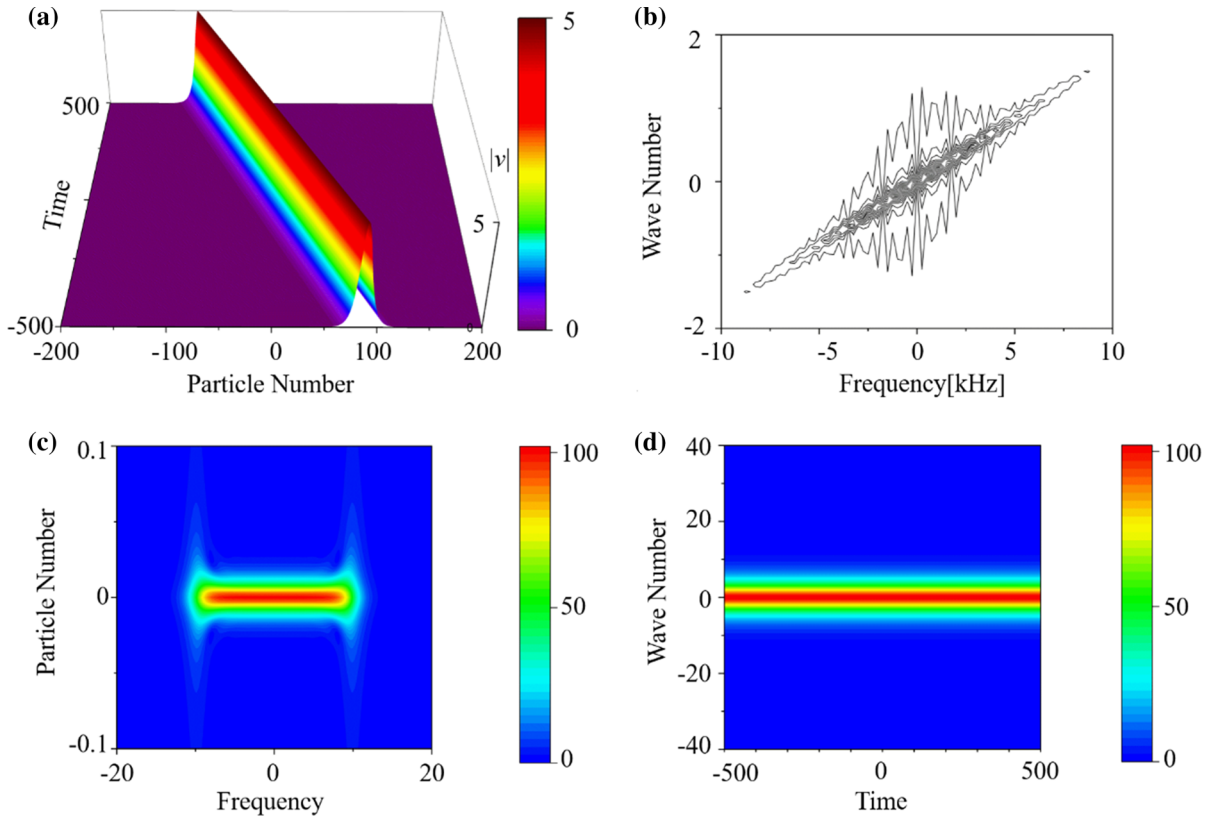

Fig. 3 **a** Evolution of the bright single-solitary wave solution, Eq. (27), in the space–time domain with $c_0 = 1$, $\gamma_0 = 0.5$, $\varepsilon = 1.2$ and $k_1 = 1$; **b** the dispersion curve corresponding to panel (**a**); **c** and **d** show the energy transfer during the dynamic evolution process in the space–frequency domain and time–wavenumber domain, respectively

low-frequency part occupies the majority and is concentrated near 0-frequecy, but the high-frequency part occupies a relatively small proportion. That is to say, the energy of the bright solitary wave is concentrated in the low-frequency domain.

Figure 4a shows the evolution of the dark single-solitary wave in the space–time domain. Most of its frequency and wavenumber are distributed near zero point, see Fig. 4b. And its evolution diagrams in the space-frequency domain [Fig. 4c] and time–wavenumber domain [Fig. 4d] show that the energy is symmetrically distributed on both sides near zero frequency or wavenumber.

In fact, Figs. 3 and 4 describe the same physical phenomenon, but in different ways. However, the dispersion curve in Fig. 4b is relatively simple. It seems clearer and more intuitive to describe the physical phenomena of solitary waves with the bright solitary waves. Thus, the following analysis will be mainly focused on the bright solitary waves.

For the complicated double-solitary wave, we consider the following two different cases: (I) $k_1 \cdot k_2 < 0$, and (II) $k_1 \cdot k_2 > 0$ by supposing $\omega_1, \omega_2 > 0$. The double-solitary wave in the former case is called the Type-I double-solitary wave, and the latter is called the Type-II double-solitary wave. As indicated in Ref. [33], the multiple solitary waves can be regarded as the interaction (or elastic collision) of single-solitary waves. Therefore, the two cases mentioned above correspond to collisions of θ_1-solitary wave and θ_2-solitary wave running in the opposite (Type-I) and the same (Type-II) directions, respectively.

Figure 5a shows the evolution of the Type-I bright double-solitary wave [Eq. (28)] in the space–time domain. It is demonstrated that the double-solitary wave can be regarded as the elastic collision of two single-solitary waves. As we know, the phase shift after the interaction of solitary waves is an important physical phenomenon [41]. However, the Type-I

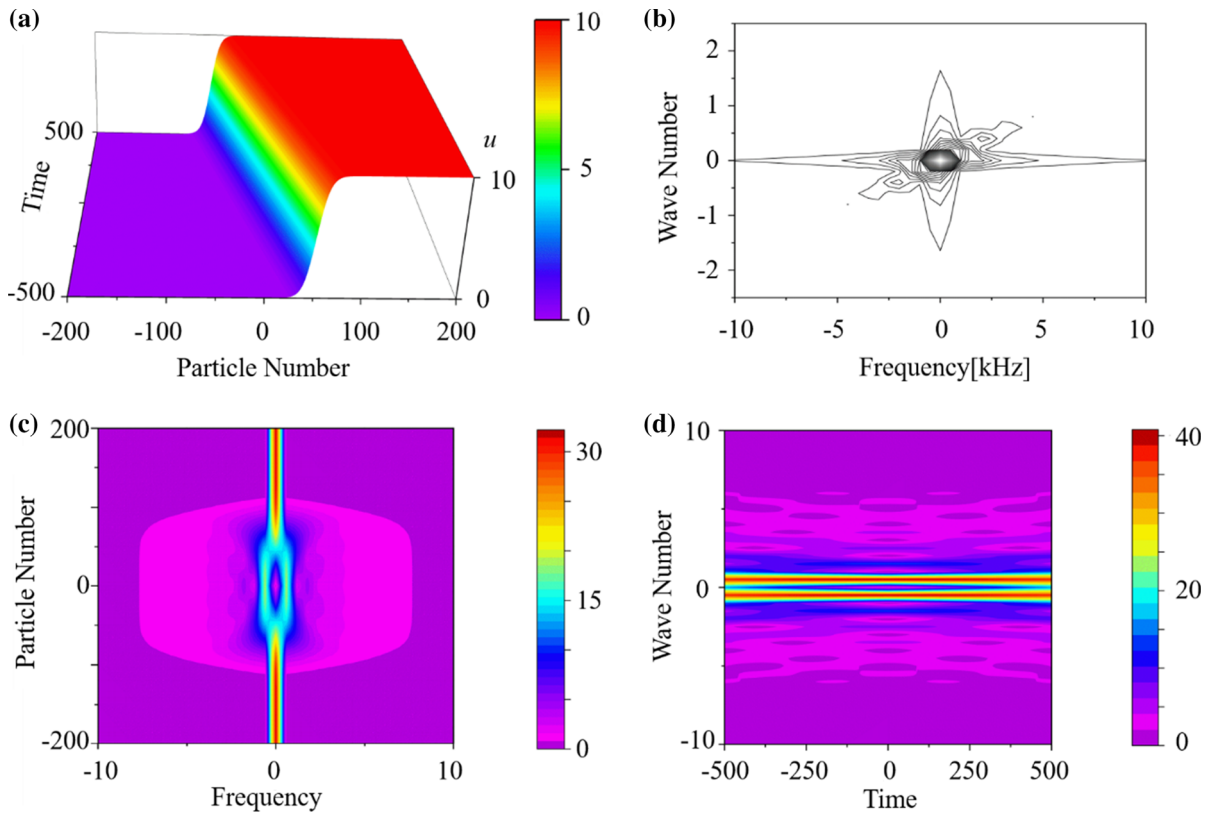

Fig. 4 **a** Evolution of the dark single-solitary wave solution Eq. (34) in the space–time domain with $c_0 = 1, \gamma_0 = 0.5, \varepsilon = 1.2$ and $k_1 = -1$; **b** the dispersion curve corresponding to panel (**a**); **c** and **d** show the energy transfer during the dynamic evolution process in the space–frequency domain and time–wavenumber domain, respectively

double-solitary wave does not present a phase shift, but exhibits a sharp peak at the center of the collision between two single-solitary waves.

Figure 5b illustrates the dispersion curves of the Type-I bright double-solitary wave corresponding to Fig. 5a. It is shown that the dispersion curves are concentrated in a cross-like region near two diagonal lines passing through the zero point. The energy transfer during the dynamic collision is shown in Fig. 5c in the space–frequency domain and in Fig. 5d in the time–wavenumber domain. Before the collision, the energy flows from high frequencies/wavenumbers to low frequencies/wavenumbers; during the collision process, the energy concentrates to the low-frequency/wavenumber region very quickly; and after the collision, the energy flows from low frequencies/wavenumbers to high frequencies/wavenumbers. For the elastic collision, the total energy is conserved.

Figure 6 shows the evolution of the Type-I dark double-solitary wave [Eq. (35)] in the space–time domain corresponding to Fig. 5. It can be seen that the waveform is very similar to a group of steps with obvious changes in amplitude.

Figure 7 shows the evolution of the Type-II bright double-solitary wave [Eq. (28)] in the space–time domain. A dip appears at the collision center of two single-solitary waves, and a significant phase shift occurs after the collision, which is similar to the solitary waves in the KdV equation (cf. Ref. [33]). The corresponding dispersion curve shown in Fig. 7b is distributed near two oblique lines passing through the zero point with a very small angle. The evolutions in the space–frequency domain [Fig. 7c] or time–wavenumber domain [Fig. 7d] show that before the collision, the energy flows from the high frequencies/wavenumbers to low frequencies/wavenumbers. During the collision process, the energy is rapidly concentrated to the low-frequency/wavenumber region. After the collision, the energy flows from the low frequencies/wavenumbers to high frequencies/

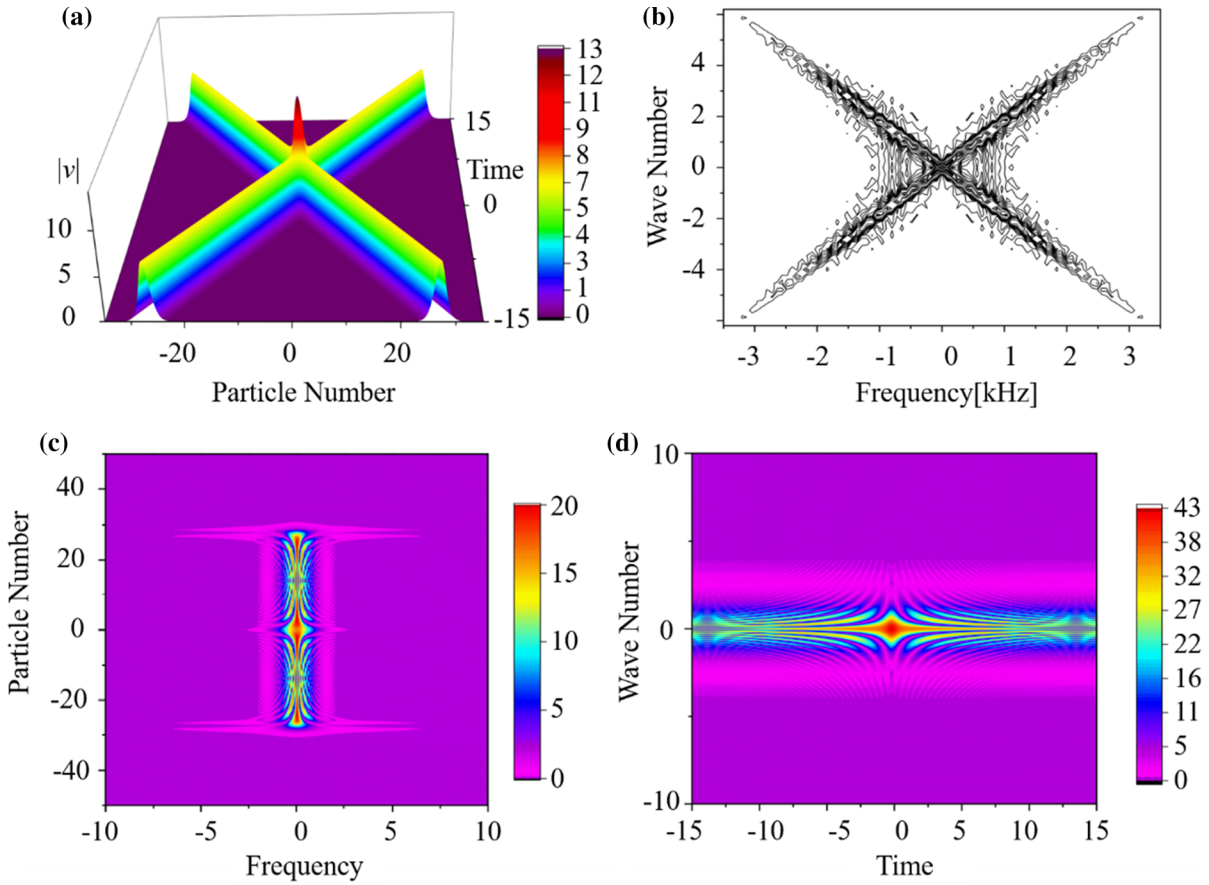

Fig. 5 **a** Evolution of the Type-I bright double-solitary wave solution, Eq. (28), in the space–time domain with $c_0 = 1$, $\gamma_0 = 0.5$, $\varepsilon = 1.2$, $k_1 = -1.5$ and $k_2 = 1.5$; **b** the dispersion curve corresponding to panel (**a**); panels (**c**) and (**d**) show the energy transfer during the dynamic collision process in the space–frequency domain and time–wavenumber domain, respectively

wavenumbers. The total energy is conserved. The Type-II dark double-solitary wave [Eq. (35)] corresponding to Fig. 7a is shown in Fig. 8. Its waveform, although exhibits steps with changes of amplitude, is obviously different from that of the Type-I dark double-solitary wave shown in Fig. 6.

Through the above analysis, we can summarize the differences between the two types of double-solitary waves: Type-I can be seen as two single-solitary waves colliding in the opposite direction (cf. Figs. 5 and 6) without phase shift, and Type-II can be regarded as two single-solitary waves colliding in the same direction (cf. Figs. 7 and 8) with a phase shift after collision.

The same method can be used to analyze the triple- and quadruple-solitary wave solutions. The results are similar and will not be presented here.

3 Numerical analysis of stability of double-solitary waves

The stability of double-solitary wave will be studied numerically by following the idea proposed in Ref. [33]. A perturbation is randomly added on the solitary wave solution as the initial condition, and then, the evolution of the solitary wave in the system is examined numerical. If the solitary wave is stable, the perturbation will gradually disappear; otherwise, the perturbation will increase exponentially with the evolution, thus destroying the waveform of solitary wave. The perturbation method has also been used in a large number of laboratory experiments [42, 43], and the experimental data are in good agreement with the simulation results.

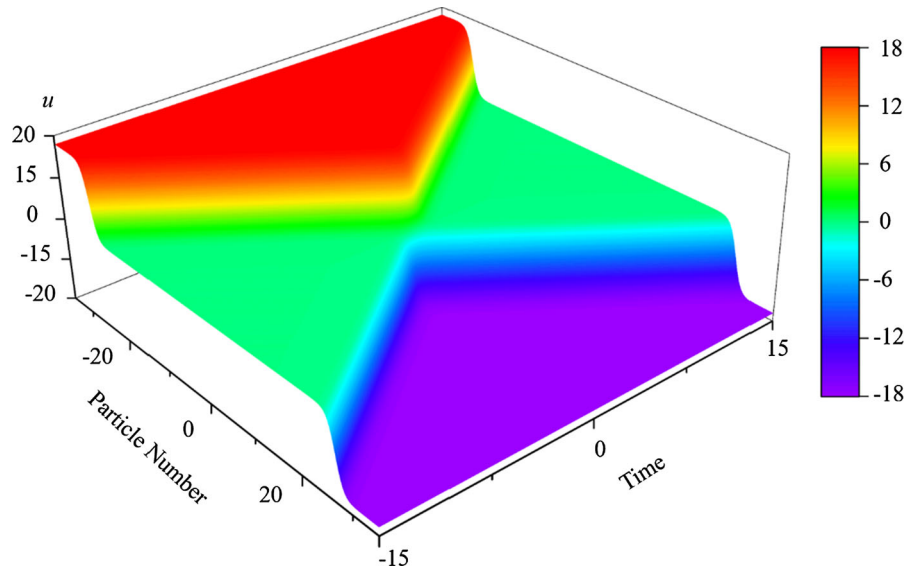

Fig. 6 Evolution of the Type-I dark double-solitary wave solution, Eq. (35), in the space–time domain with $c_0 = 1$, $\gamma_0 = 0.5$, $\varepsilon = 1$, $k_1 = -1.5$ and $k_2 = 1.5$

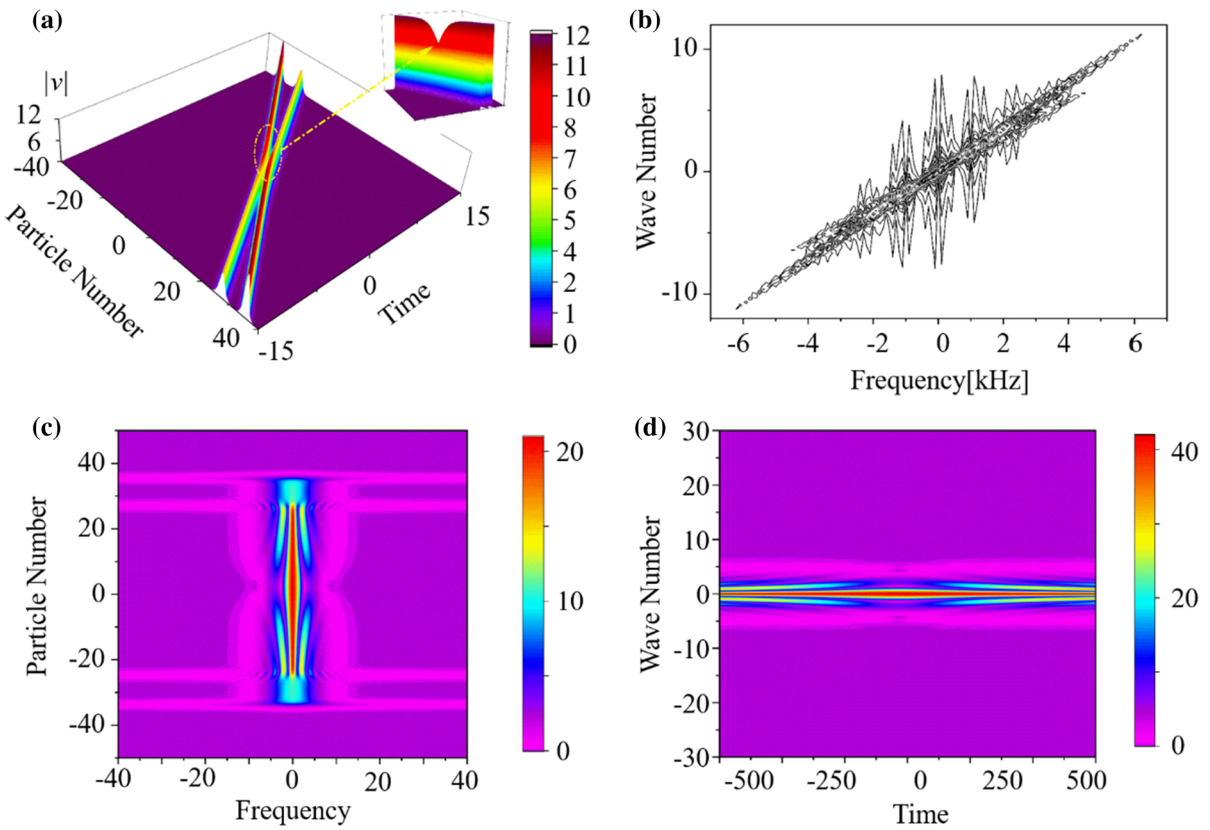

Fig. 7 **a** Evolution of the Type-II bright double-solitary wave solution, Eq. (28), in the space–time domain with $c_0 = 1$, $\gamma_0 = 0.5$, $\varepsilon = 1$, $k_1 = 2$ and $k_2 = 1.5$; **b** the dispersion curve corresponding to panel (**a**); panels **c** and **d** show the energy transfer during the dynamic collision process in the space–frequency domain and time-wavenumber domain, respectively

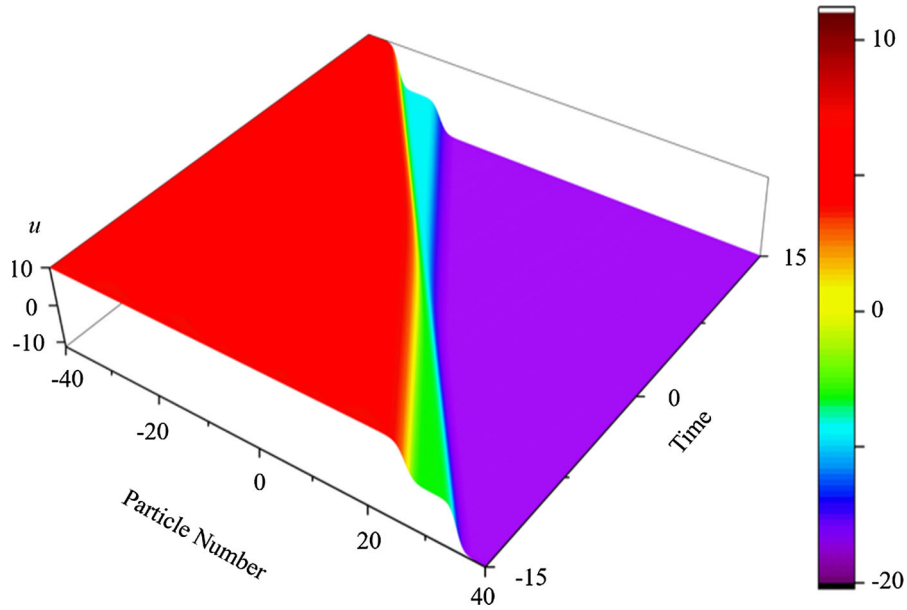

Fig. 8 Evolution of the Type-II dark double-solitary wave, Eq. (35), in the space–time domain with $c_0 = 1$, $\gamma_0 = 0.5$, $\varepsilon = 1$, $k_1 = 2$ and $k_2 = 1.5$

Here we consider the collision of the following two dark single-solitary waves running in the opposite directions:

$$10\tanh[-(x-40)+t] \text{ and } 10\tanh[-(x-50)-t], \tag{38}$$

which, according to the previous analysis, should generate the following Type-I dark double-solitary wave:

$$u_2(x,t) = 20\frac{\mathrm{e}^{-x+t+40} + \mathrm{e}^{-x-t+50} + 40\mathrm{e}^{-2x+90}}{1 + \mathrm{e}^{-x+t+40} + \mathrm{e}^{-x-t+50} - 20\mathrm{e}^{-2x+90}} - 20. \tag{39}$$

To examine the evolution stability of the dark double-solitary wave, we use the fourth-order Runge–Kutta method to solve Eq. (4) numerically by assuming an initial excitation which is the displacement field from Eq. (38) at time $t = 0$ with a uniformly distributed random perturbation of amplitude 10^{-4} [41–44]. The nondimensionalized time step in computation is 10^{-3}.

Figure 9 shows a comparison between the collision stability analysis of two dark single-solitary waves running in the opposite directions with the same wave velocities governed by Eq. (4) and the corresponding space–time evolution of Eq. (39) with the same parameters. The evolution of the dark double-solitary wave solution obtained from the Runge–Kutta method is demonstrated in Fig. 9a with $\delta_0 = 10^{-3}$. The results show that the waveforms of the two single-solitary waves remain stable, and the characteristics remain unchanged. At $t = 700$, the two single-solitary waves collide and then return to the state before collision. From the point of view of the whole dynamic process, the two single-solitary waves successfully excite a stable dark double-solitary wave. The space–time evolution of the double-solitary wave shown in Eq. (39) is illustrated in Fig. 9b with the same parameters as in Fig. 9a. The similarity of Fig. 9a and b implies that the solitary wave in Fig. 9a is the Type-I double-solitary wave.

In order to study the influence of velocity on the stability of solitary wave collision, we consider the collision of the following two dark single-solitary waves with different velocities:

$$10\tanh[-(x-55)+2t] \text{ and } 10\tanh[-(x-45)-t], \tag{40}$$

which, according to the previous analysis, should generate the following Type-I dark double-solitary wave:

$$u_2(x,t) = 20\frac{\mathrm{e}^{-x+2t-55} + \mathrm{e}^{-x-t+45} + 40\mathrm{e}^{-2x+t+100}}{1 + \mathrm{e}^{-x+2t-55} + \mathrm{e}^{-x-t+45} - 20\mathrm{e}^{-2x+t+100}} - 20. \tag{41}$$

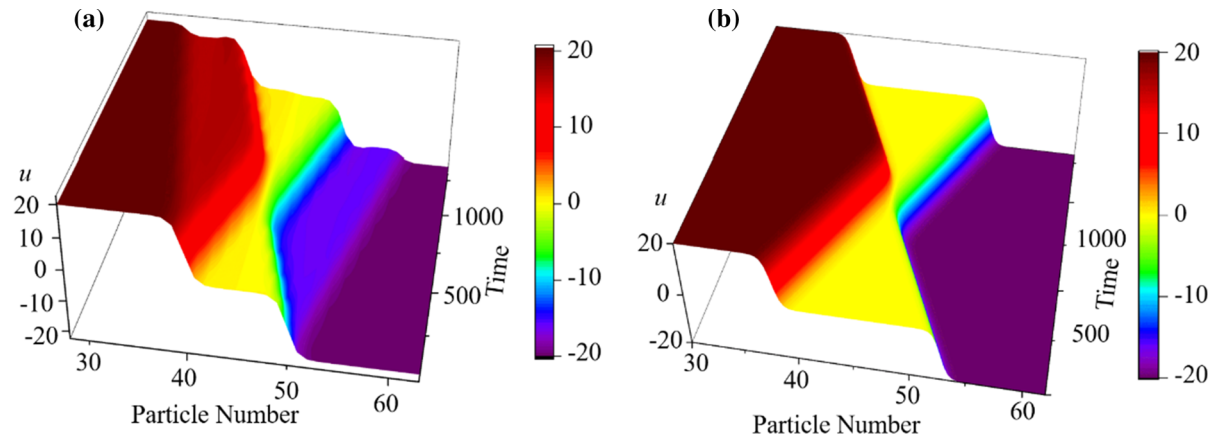

Fig. 9 **a** Collision stability analysis of two dark single-solitary waves with the same velocity running in the opposite directions governed by Eq. (4) with $\delta_0 = 10^{-3}$, and **b** the space–time evolution of the Type-I dark double-solitary wave [Eq. (39)] with the same parameters as in panel (**a**)

Following the same process as above analysis, we solve Eq. (4) numerically using the fourth-order Runge–Kutta method with the initial excitation from the perturbed initial values of Eq. (40). Comparison between the collision stability analysis of two dark single-solitary waves running in the opposite directions with the different wave velocities governed by Eq. (4) is shown in Fig. 10a, and the corresponding space–time evolution of Eq. (41) with the same parameters is illustrated in Fig. 10b. It is seen from both Fig. 10a and b that the waveforms of the two single-solitary waves are well preserved before the collision, and the perturbation is not amplified. At $t = 700$, the two solitary waves collide, and the perturbation increases exponentially. After the collision, the waveform of the solitary wave becomes distorted obviously. Therefore, the collision is unstable, and the excited double-solitary wave are also unstable. Comparing these two figures, we find that the solitary wave in Fig. 10a shows the Type-I dark double-solitary wave, but it is not convergent and is unstable.

Further numerical tests show that the generated double-solitary wave can propagate stably for a longer time (i.e., the life span becomes longer [45]) if the velocity difference of two single-solitary waves are smaller. This is an interesting phenomenon in granular phononic crystals. It seems that only the opposite collision between two single-solitary waves with the same velocities, as shown in Fig. 9, is stable.

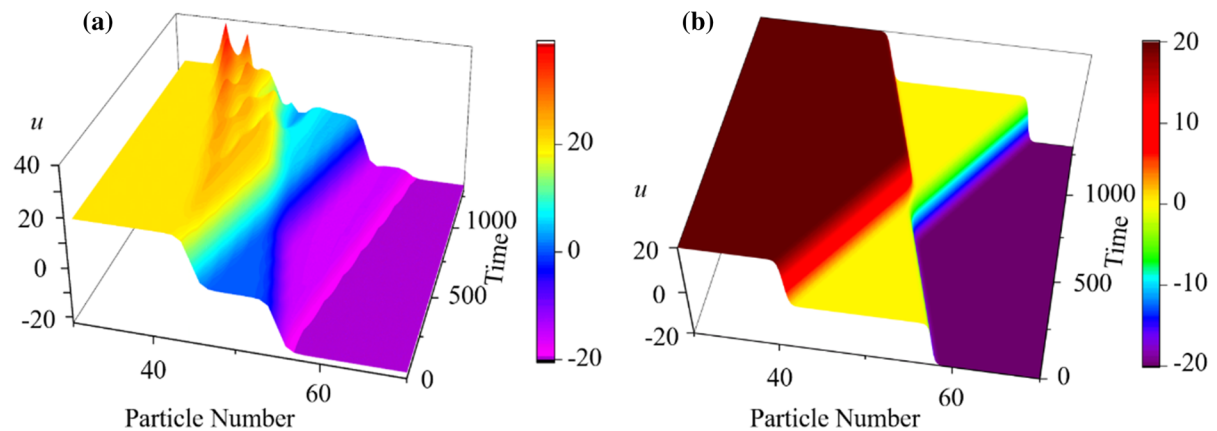

Fig. 10 Collision stability analysis of two dark single-solitary waves with different wave velocities running in the opposite directions governed by Eq. (4) with $\delta_0 = 10^{-3}$, and (**b**) the space–time evolution of Eq. (41) with the same parameters as in (**a**)

Next, we check the stability of the Type-II dark double-solitary wave by solving Eq. (4) with $\delta_0 = 10^{-3}$ using the fourth-order Runge–Kutta method.

Figure 11 shows the stability analysis of a Type-II double-solitary wave solution by Eq. (4) with $\delta_0 = 10^{-3}$. The data from the Type-II double-solitary wave shown in Fig. 8 at a certain time are used as the input signal (see Fig. 11a). The perturbation magnitude of 10^{-4} is added to the signal. Figure 11b shows that a double-solitary wave is excited in the original system before $t = 1000$, and the waveform keeps good. But after $t = 1000$, the perturbation is amplified exponentially, and the waveform loses the characteristics of the solitary wave. It is obvious that the Type-II double-solitary wave is unstable. Further numerical calculations support this conclusion although we cannot exhaust all cases.

Collision of moving solitary waves is an interesting phenomenon which is closely related to the stability of the single-solitary waves. However, our analytical solutions and corresponding numerical simulations show that the stability of collision is related to the stability of double-solitary waves. In other words, only when there is a stable double-solitary wave, the collision of two single-solitary waves is stable.

Next, we will present qualitative analysis about the stability of multiple solitary waves from the point of view of geometry.

4 Qualitative analysis of stability of multiple solitary waves

According to the analysis in Section III, the multiple solitary waves can be regarded as (or equivalently be excited by) the dynamic interaction (collision) of single-solitary waves. We first consider the case of a double-solitary wave. The two kinds of double-solitary waves (Type-I and Type-II) can be schematically illustrated in Fig. 12 where the strips represent the peak regions of the bright single-solitary waves or the rapid-changing regions of the dark single-solitary waves. In the other regions, (I)–(IV), the amplitude tends to zero/constant for the bright/dark double-solitary wave. So, except in the strongly interacting regions marked by area S, the double-solitary wave can be regarded approximately as the superposition of two single-solitary waves (also refer to Ref. [33]). In the strongly interacting region, the two solitary waves interact sufficiently and generate intense energy exchange and flow. We find that bigger the area is, the longer the running time of the simulation program is. Thus, it is reasonable to infer that the stability of the double-solitary wave is relevant to the area of the strongly interacting region, and the smaller the area is, the more stable the system is.

The area of the strongly interacting region is

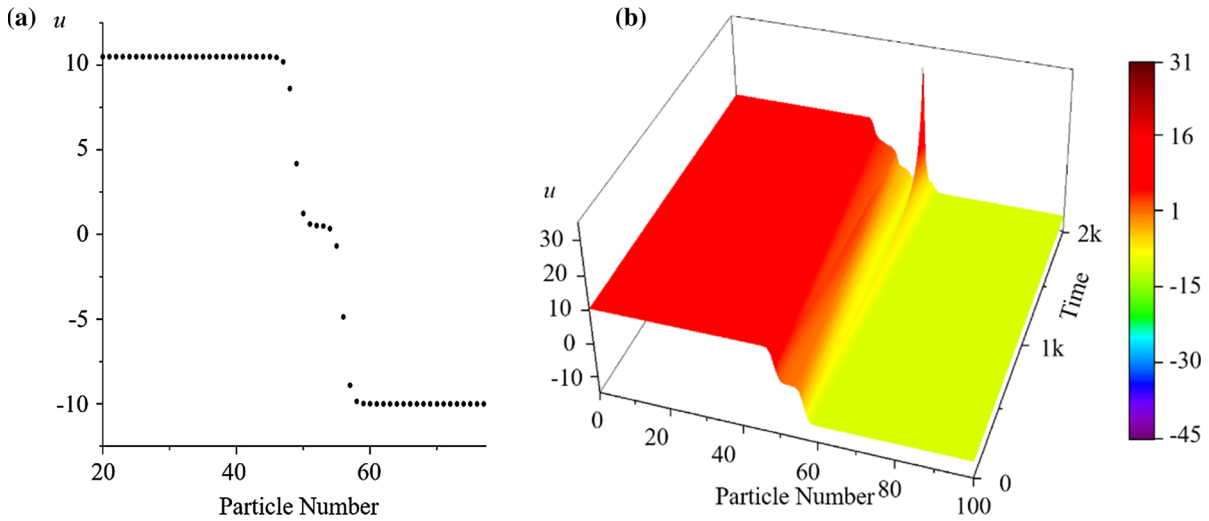

Fig. 11 Numerical simulation of evolution of a Type-II double-solitary wave solution by Eq. (4) with $\delta_0 = 10^{-3}$: **a** The profile of Type-II double-solitary wave solution from Fig. 8 at $t = -23$, and **b** evolution of the solution with the initial condition from panel (**a**) with a perturbation

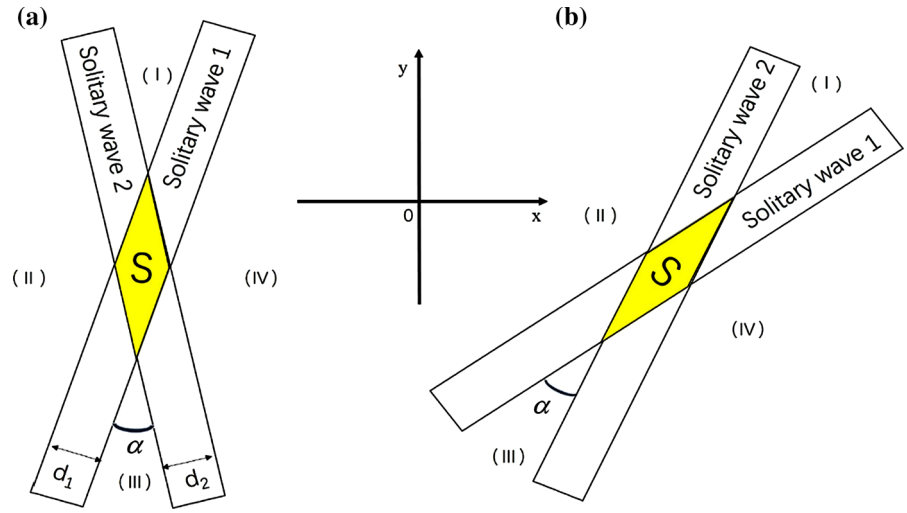

Fig. 12 Schematic diagrams of two kinds of double-solitary waves excited by the interaction (collision) of two single-solitary waves: (**a**) Type-I, and (**b**) Type-II. The yellow intersection regions marked by area S represent the strong-interaction regions. The phase shift is neglected in (**b**) because it does not affect the interaction of solitary waves

$$S = \frac{d_1 d_2}{\sin \alpha}, \tag{35}$$

where α $(0 < \alpha \leq 90^\circ)$ is the angle between the two single-solitary waves; and d_1 and d_2 are the effective widths of the single-solitary waves. It is easy to see that S is a monotone decreasing function of α with the minimum value of $S_{\min} = d_1 d_2$ when $\alpha = 90^\circ$. If the double-solitary wave is stable at an angle smaller than α, then it is also stable at the angle α. The bigger the angle α is, the smaller the area S is, and therefore the more stable the double-solitary wave is. $\alpha = 90^\circ$ yields the minimum S. The Type-I double-solitary wave includes the case of $\alpha = 90^\circ$, which means it may be stable. It is obvious that the angle α of Type-II double-solitary wave is smaller than that of Type-I and is generally much smaller than 90°. Therefore, the Type-II double-solitary wave is generally unstable.

It is worth noting that the width of solitary waves is the diameter of five spheres [32]. Since the space width of solitary wave is also determined after the sphere chain is selected, we ignore the influence of the width of solitary wave on the stability when we consider its geometric structure.

Next, we consider the case of a triple-solitary wave which can be treated as the dynamic interaction of three single-solitary waves.

Figure 13 shows a schematic diagram for dynamic analysis of triple-solitary waves which can also be regarded as the interaction between double-solitary waves and single-solitary waves. There are two situations: one single-solitary wave propagates against the other two (or one double-solitary wave) as shown in Fig. 13a, and all three single-solitary waves (or one single-solitary wave and one double-solitary wave) propagate in the same direction as shown in Fig. 13b. In both situations, we will definitely have two single-solitary waves propagating in the same direction. And the above analysis demonstrates that the collision of these two single-solitary waves generates an unstable Type-II double-solitary wave. Therefore, the triple-solitary wave is generally unstable. Indeed, we could not find a stable triple-solitary wave through many numerical tests.

Similarly, a multiple solitary wave with the order higher than three is generally unstable.

5 Conclusions

In this paper, the analytical solutions of multiple solitary waves in a pre-compressed spherical chain are derived based on the homogeneous balance principle and bilinear method in the long-wave approximation. The dynamic behavior and stability of the double-solitary waves are studied in detail. The main results and conclusions may be summarized as follows:

(1) The present solutions show that the multiple solitary waves can be regarded as the dynamic interaction (collision) of multiple single-solitary waves. The obtained solutions have the same form those constructed through the inspiration of the solutions to the KdV system. However, a

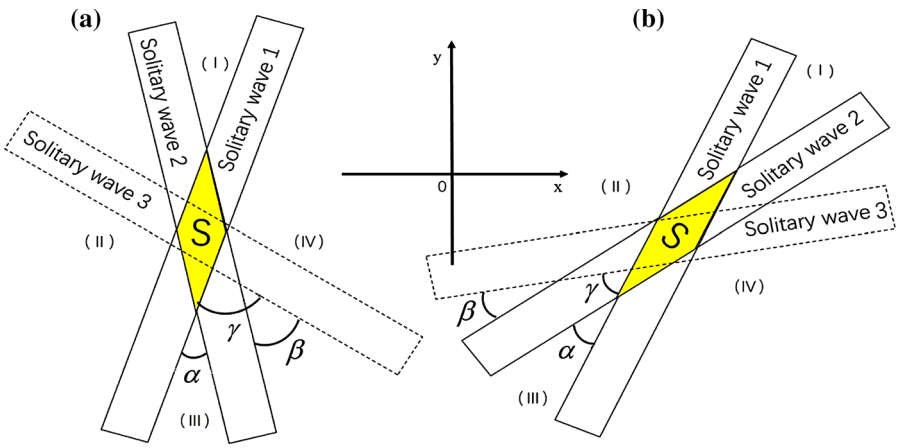

Fig. 13 Schematic diagrams of triple-solitary waves excited by the interaction of a stable single-solitary wave and a stable double-solitary wave: (**a**) single-solitary wave 1 propagates against 2 and 3; (**b**) all three single-solitary waves propagate in the same direction

great difference between the present solutions and those from the KdV system appears when the wavenumbers of arbitrary two single-solitary waves are opposite (i.e., when $k_i = -k_j$ in Eq. (34)). This implies that the KdV system cannot exactly capture the nature of the original granular system.

(2) The detailed analysis of the double-solitary wave which is interpreted as collision of two single-solitary waves is provided. Different dynamic behaviors depending on the collision directions are exhibited. The opposite collision does not show any phase shift and may generate a stable double-solitary wave, and it is contrary for the collision in the same direction. In this way, we divide the double-solitary wave into two categories which are termed as Type-I (opposite collision) and Type-II. Numerical simulation shows a stable Type-I double-solitary wave. Other high-order multiple solitary waves can be analyzed in the similar way.

(3) The strongly nonlinear interaction between single-solitary waves takes place in a small spatiotemporal region. We argue that the smaller this region is, the more likely the system is to be stable. This provides a possible way to determine the stability of multiple solitary waves qualitatively.

It should be mentioned that the numerical instead of the analytical perturbation method is applied for stability analysis of solitary waves because of the complexity of the problem. One disadvantage of the numerical method is that it can only examine the stability of the system in the period of the simulated evolution. Obviously, we cannot simulate the evolution in an infinite time period.

Although we argue that a stable multiple solitary waves with the order higher than three is much impossible to exist in a pre-compressed identical spherical chain. However, it does not mean that it cannot exist in a polyatomic ball chain. It should be an interesting topic to study multiple solitary waves and even chaos [46, 47] in polyatomic granular crystals and granular metamaterials.

Acknowledgements This piece of work is supported by the National Natural Science Foundation of China under grant numbers 11532001 and 11991031. The third author (Y. S. Wang) is also grateful for the support of National Natural Science Foundation of China under grant number 12021002.

Declaration

Conflict of interest We would like to declare on behalf of our co-authors that the work described in this paper is original, has not been published previously, and is not considered for publication elsewhere, in whole or in part. All the authors listed have approved the submission of the manuscript. No conflict of interest exits in the submission of the manuscript.

Code availability The datasets used or analyzed during the current study are available from the corresponding author on reasonable request.

References

1. Kittel, C.: Introduction to Solid State Physics. Wiley, New York (2004)
2. Jayaprakash, K.R., Starosvetsky, Y., Vakakis, A.F., Peeters, M., Kerschen, G.: Nonlinear normal modes and band zones

in granular chains with no pre-compression. Nonlinear Dyn. **63**, 359–385 (2011)
3. Pennec, Y., Djafari-Rouhani, B., Vasseur, J.O., Khelif, A., Deymier, P.A.: Tunable filtering and demultiplexing in phononic crystals with hollow cylinders. Phys. Rev. E **69**, 4 (2004)
4. Khelif, A., Choujaa, A., Benchabane, S., Djafari-Rouhani, B., Laude, V.: Guiding and bending of acoustic waves in highly confined phononic crystal waveguides. Appl. Phys. Lett. **84**, 4400 (2004)
5. Hsiao, F.-L., Khelif, A., Moubchir, H., Choujaa, A., Chen, C.-C., Laude, V.: Waveguiding inside the complete band gap of a phononic crystal slab. Phys. Rev. E **76**, 056601 (2007)
6. Wang, Y., Yousefzadeh, B., Chen, H., Nassar, H., Huang, G., Daraio, C.: Observation of nonreciprocal wave propagation in a dynamic phononic lattice. Phys. Rev. Lett. **121**, 194301 (2018)
7. Chen, Y., Wu, B., Su, Y., Chen, W.Q.: Tunable two-way unidirectional acoustic diodes: design and simulation. J. Appl. Mech. **86**(3), 031010 (2019)
8. Zhou, W.J., Li, X.P., Wang, Y.S., Chen, W.Q., Huang, G.L.: Spectro-spatial analysis of wave packet propagation in nonlinear acoustic metamaterials. J. Sound Vib. **413**, 250 (2018)
9. Pennec, Y., Djafari-Rouhani, B., Vasseur, J.O., Khelif, A., Deymier, P.A.: Tunable filtering and demultiplexing in phononic crystals with hollow cylinders. Phys. Rev. E **69**, 046608 (2004)
10. Casadei, F., Delpero, T., Bergamini, A., Ermanni, P., Ruzzene, M.: Piezoelectric resonator arrays for tunable acoustic waveguides and metamaterials. J. Appl. Phys **112**, 064902 (2012)
11. Wang, Y.F., Wang, Y.Z., Wu, B., Chen, W.Q., Wang, Y.S.: Tunable and active phononic crystals and metamaterials. Appl. Mech. Rev **72**(4), 040801 (2020)
12. Daraio, C., Nesterenko, V.F., Herbold, E.B., Jin, S.: Tunability of solitary wave properties in one-dimensional strongly nonlinear phononic crystals. Phys. Rev. E **73**, 026610 (2006)
13. Chaunsali, R., Theocharis, G.: Self-induced topological transition in phononic crystals by nonlinearity management. Phys. Rev. B **100**, 014302 (2019)
14. Daraio, C., Nesterenko, V., Herbold, E., Jin, S.: Strongly nonlinear waves in a chain of Teflon beads. Phys. Rev. E **72**, 016603 (2005)
15. Ganesh, R., Gonella, S.: From modal mixing to tunable functional switches in nonlinear phononic crystals. Phys. Rev. Lett. **114**, 054302 (2015)
16. Boechler, N., Theocharis, G., Job, S., Kevrekidis, P.G., Porter, M.A., Daraio, C.: Discrete breathers in one-dimensional diatomic granular crystals. Phys. Rev. Lett. **104**, 244302 (2010)
17. Lin, W.H., Daraio, C.: Wave propagation in one-dimensional microscopic granular chains. Phys. Rev. E **94**, 052907 (2016)
18. Chong, C., Porter, M.A., Kevrekidis, P.G., Daraio, C.: Nonlinear coherent structures in granular crystals. J. Phys. Condensed Matter **29**, 413003 (2017)
19. Molerón, M., Chong, C., Martónez, A.J., Porter, M.A., Kevrekidis, P.G., Daraio, C.: Nonlinear excitations in magnetic lattices with long-range interactions. New J. Phys. **21**, 063032 (2019)
20. Singhal, T., Kim, E., Kim, T.Y., Yang, J.: Weak bond detection in composites using highly nonlinear solitary waves. Smart Mater. Struct. **26**, 055011 (2017)
21. Porter, M.A., Daraio, C., Herbold, E.B., Szelengowicz, I., Kevrekidis, P.G.: Highly nonlinear solitary waves in periodic dimer granular chains. Phys. Rev. E **77**, 015601(R) (2008)
22. Yang, J., Silvestro, C., Khatri, D., De Nardo, L., Daraio, C.: Interaction of highly nonlinear solitary waves with linear elastic media. Phys. Rev. E **83**, 046606 (2011)
23. Burgoyne, H.A., Newman, J.A., Jackson, W.C., Daraio, C.: Guided impact mitigation in 2D and 3D granular crystals. Procedia Eng. **103**, 52 (2015)
24. Ciampa, F., Mankar, A., Marini, A.: Phononic crystal waveguide transducers for nonlinear elastic wave sensing. Sci. Rep. **7**, 14712 (2017)
25. Kurosu, M., Hatanaka, D., Onomitsu, K., Yamaguchi, H.: On-chip temporal focusing of elastic waves in a phononic crystal waveguide. Nat. Commun **9**, 1331 (2018)
26. Nesterenko, V.F.: Dynamics of Heterogeneous Materials. Springer, New York (2001)
27. Fermi, E., Pasta, J., Ulam, S.: Studies of Nonlinear Problems, pp. 977–988. University of Chicago Press, Chicago (1955)
28. Lamb, G.L., Jr.: Elements of Soliton Theory. Wiley, New York (1980)
29. Li, Q., Pnevmatikos, S., Economou, E., Soukoulis, C.: Lattice-soliton scattering in nonlinear atomic chains. Phys. Rev. B **37**(7), 3534 (1988)
30. Nayfeh, A.H., Mook, D.T.: Nonlinear Oscillations. Wiley, New York (1979)
31. Schiesser, W.E.: Spline Collocation Methods for Partial Differential Equations with Applications in R. Wiley, USA (2017)
32. Nesterenko, V. F.: Propagation of nonlinear compression pulses in granular media. Prikl. Mekh. Tekh. Fiz. 24, 136 (1983) [J. Appl. Mech. Phys. 24, 733 (1983)]
33. Liu, Z.G., Wang, Y.S., Huang, G.L.: Solitary waves in a granular chain of elastic spheres: multiple solitary solutions and their stabilities. Phys. Rev. E **99**, 062904 (2019)
34. Hirota, R.: The Direct Method in Soliton Theory. Cambridge University Press, New York (2004)
35. Wang, M.L.: Exact solutions for a compound KdV-Burgers equation. Phys. Lett. A **213**, 279 (1996)
36. Wang, M.L., Zhou, Y., Li, Z.B.: Application of a homogeneous balance method to exact solutions of nonlinear equations in mathematical physics. Phys. Lett. A **216**, 67 (1996)
37. Zhang, J.L., Liu, Z.G., Li, S.W., Wang, M.L.: Solitary waves and stable analysis for the quintic discrete nonlinear Schrödinger equation. Phys. Scripta **86**, 015401 (2012)
38. Zhang, J.L., Liu, Z.G.: Exact solutions of discrete complex cubic Ginzburg—Landau equation and their linear stability. Commun. Theor. Phys. **56**, 1111 (2011)
39. Hietarinta, J.: Exact solution of the Korteweg—de Vries equation for multiple collisions of solitons. Phys. Rev. Lett. **27**, 1192 (1971)
40. Wang, M, L.: Nonlinear Evolution Equations and Solitons, Lanzhou University Press, Lanzhou (1990) (**in Chinese**)

41. Lautrup, B., Appali, R., Jackson, A.D., et al.: The stability of solitons in biomembranes and nerves. Eur. Phys. J. E **34**, 57 (2011)
42. Kevrekidis, P.G.: The Discrete Nonlinear Schrödinger Equation. Springer, Berlin (2009)
43. Trill, S., Torruellas, W.: Spatial Solitons, 1st edn. Springer, Berlin (2001)
44. Agrawal, G.P.: Nonlinear Fiber Optics. Academic, New York (1995)
45. Ta-Tsien, L., Yi, Z., De-Xing, K.: Global classical solutions for general quasilinear hyperbolic systems with decay initial data. Nonlin. Anal. **28**, 1299 (1997)
46. Wu, Q.L., Qi, G.Y.: Homoclinic bifurcations and chaotic dynamics of non-planar waves in axially moving beam subjected to thermal load. Appl. Math. Modell. **83**, 674 (2020)
47. Seydel, R.: Practical Bifurcation and Stability Analysis. Springer, New York (2010)